



## Structure and vibrational modes of AgI-doped AsSe glasses: Raman scattering and *ab initio* calculations

O. Kostadinova<sup>a,1</sup>, A. Chrissanthopoulos<sup>a,b</sup>, T. Petkova<sup>c</sup>, P. Petkov<sup>d</sup>, S.N. Yannopoulos<sup>a,\*</sup>

<sup>a</sup> Foundation for Research and Technology Hellas, Institute of Chemical Engineering and High Temperature Chemical Processes, P.O. Box 1414, Patras GR-26504, Greece

<sup>b</sup> Department of Chemistry, University of Patras, Patras GR-26504, Greece

<sup>c</sup> Institute of Electrochemistry and Energy Systems (IEES), Bulgarian Academy of Sciences, Sofia, Bulgaria

<sup>d</sup> Laboratory of Thin Film Technology, Department of Physics, University of Chemical Technology and Metallurgy, Sofia, Bulgaria

### ARTICLE INFO

#### Article history:

Received 28 September 2010

Received in revised form

13 December 2010

Accepted 19 December 2010

Available online 28 December 2010

#### Keywords:

Chalcohalide glasses

Raman scattering

*Ab initio* calculations

Glass structure

Short-range order

### ABSTRACT

We report an investigation of the structure and vibrational modes of  $(\text{AgI})_x(\text{AsSe})_{100-x}$ , bulk glasses using Raman spectroscopy and first principles calculations. The short- and medium-range structural order of the glasses was elucidated by analyzing the reduced Raman spectra, recorded at off-resonance conditions. Three distinct local environments were revealed for the AsSe glass including stoichiometric-like and As-rich network sub-structures, and cage-like molecules ( $\text{As}_4\text{Se}_n$ ,  $n=3, 4$ ) decoupled from the network. To facilitate the interpretation of the Raman spectra *ab initio* calculations are employed to study the geometric and vibrational properties of  $\text{As}_4\text{Se}_n$  molecular units that are parts of the glass structure. The incorporation of AgI causes appreciable structural changes into the glass structure. AgI is responsible for the population reduction of molecular units and for the degradation of the As-rich network-like sub-structure via the introduction of As–I terminal bonds. *Ab initio* calculations of mixed chalcohalide pyramids  $\text{AsSe}_m\text{I}_{3-m}$  provided useful information augmenting the interpretation of the Raman spectra.

© 2010 Elsevier Inc. All rights reserved.

### 1. Introduction

Chalcogenide glasses (ChGs) have proved a very fertile field of experimental and theoretical research over the last 30 years due to several applications of these materials, which are the outcome of an impressive variety of athermal photoinduced phenomena [1]. Among the most promising applications of chalcogenide glasses doped with mobile metals (Ag, Cu) and metal halogens (AgI, CuI) is their potential use as superionic conductors and chemical sensors [2]. The fact that these amorphous inorganic materials can be easily prepared in bulk or thin film form is a major advantage. Further, ChGs exhibit enhanced chemical stability to environmental conditions and their physical properties can be fine tuned by varying the glass composition; these are characteristic features exploitable in applications [3]. Understanding details of the short- and medium-range structural order of a glassy material is essential for advancing structure–properties correlations. Vibrational spectroscopy, and in particular Raman scattering, is a very powerful experimental tool, which

is frequently employed in structural investigations of glasses [4,5]. In addition, first principles calculations and *ab initio* molecular dynamics studies [6] of structure and vibrational properties are of paramount importance in understanding the very complex, broad experimental Raman spectra and hence elucidating the nature of structural units in glasses.

Despite some progress in the field [7(a)], no systematic studies exist up to now that provide a structural rationale for the role of the ChG matrix structure and of the doping extent of the superionic additive (AgI) on the electrical or sensing properties of the material. This is partly due to the complex structure of these multi-component glasses that are difficult to analyze by classic diffraction methods in view of the high number of the partial pair distributions. Besides, micro-phase separation effects take place frequently in Ag-doped [7(b)] or AgI-doped [7(a)] ChGs, which is often overlooked and further complicates their study. To understand structure–properties relations one has to study materials that can form glasses over a wide range of compositions and various doping levels. The binary system  $\text{As}_x\text{Se}_{100-x}$  offers this possibility because it can be prepared in glassy form for a wide range of compositions exceeding the stoichiometric threshold for  $x_{\text{As}}=40$ , reaching eventually up to  $x_{\text{As}}=70$  [4]. The interest in glasses with high As content, e.g.  $x_{\text{As}}=50$  lies in the fact that a large density of homonuclear As–As bonds exist in the structure of such glasses, which are important for a variety of photoinduced

\* Corresponding author.

E-mail address: [sny@iceht.forth.gr](mailto:sny@iceht.forth.gr) (S.N. Yannopoulos).

<sup>1</sup> Present address: Laboratory of Advanced Materials Research, Department of Silicate Technology, University of Chemical Technology and Metallurgy, Sofia, Bulgaria.

effects occurring upon near-bandgap light irradiation [8]. As stated above, knowledge of the atomic arrangement is the prerequisite to understanding macroscopic properties and to develop tailor-made materials. Therefore, the present investigation is focused on the structural features and vibrational properties of  $(\text{AgI})_x(\text{AsSe})_{100-x}$ ,  $0 \leq x \leq 30$  mol%, bulk glasses using off-resonance Raman spectroscopy and *ab initio* calculations. Due to the species-specific nature of vibrational modes, Raman scattering offers unique capability for a detailed description of the glass structure over conventional diffraction methods that probe mean coordination numbers. This is particularly true in studies of glasses with complex structure containing both a network-like backbone and molecular units decoupled from the network, as is the present case.

## 2. Material and methods

### 2.1. Experimental details

The bulk materials with compositions  $\text{AgI}_x(\text{AsSe})_{100-x}$  have been prepared by a two-stage synthesis: (i) the preparation of the binary AsSe compound from elemental As and Se with 5 N purity (Alfa Aesar); (ii) the synthesis of quasi binary alloys AgI and AsSe from the obtained arsenic selenide glass and commercial AgI (Alfa Aesar). Appropriate amounts of the elements or compounds were sealed in quartz ampoules evacuated to  $\sim 10^{-3}$  Pa, and were melted in a rotary furnace. The temperature was kept constant above the liquidus of the mixture, while the melt was continuously stirred for better homogenization. The glasses were obtained by quenching melts in cold water. Raman spectra were recorded with the aid of a Fourier transform (FT) Raman spectrometer (model FRA 106/S, Bruker) using the 1064 nm laser line as the excitation source in order to meet off-resonance conditions and hence to avoid undesired photoinduced effects. The signal was detected by a liquid-nitrogen-cooled CCD (Ge-detector). The laser power was set at 150 mW to avoid heat-induced effects. The number of accumulations was 100 and the resolution was  $2 \text{ cm}^{-1}$  in order to obtain smooth, high resolution spectra.

### 2.2. Theoretical/calculation details

The Hartree–Fock (HF) molecular orbital theory as implemented in the GAUSSIAN 03 program package was utilized in the present study in order to calculate the structural details and the vibrational frequencies of two cage-like molecular units  $\text{As}_4\text{Se}_n$  ( $n=3, 4$ ) and of the chalcogenide structural models (pyramidal units)  $\text{AsI}_m(\text{SeH})_{3-m}$ ,  $m=0, 1, 2, 3$ . The accuracy of the computational method and the basis sets, which have been chosen for the investigated systems, have been tested by comparing the calculated properties with other theoretical and experimental structural data that are available in the literature. The electronic structure of the atoms participating in the investigated structures is described by the Ahlrichs TZV basis sets [9(a)]. For a more accurate description of the nature of the chemical bond between atoms and for a better determination of the vibrational energies, a polarization d-Gaussian-type function (GTF) has been added on arsenic and selenium basis set [10]. The electronic structure of the atoms participating in the iodine-containing structures are described by the double-zeta-split-valence+polarization (DZVP) basis sets [9(b)]. The basis sets are taken from Ref. [10]. The geometries of all structural models have been fully optimized at the HF level of theory.

## 3. Results

The quantitative analysis of Raman spectra, in order to get insight about the nature and population of structural units that compose the short- and medium-range structural order, necessitates the use of the so-called *reduced representation*. The reduction considers the distortion of the experimental Raman spectra that has taken place in view of the finite sample temperature and the wavelength dependence of the scattered light. Therefore, the reduced Raman spectrum represents the vibrational density of states weighted by the Raman coupling coefficient. The Stokes-side reduced Raman intensity ( $I^{\text{red}}$ ) is related to the experimentally measured one ( $I^{\text{exp}}$ ) via the equation, for details see [5]:

$$I^{\text{red}}(\tilde{\nu}) = (\tilde{\nu}_0 - \tilde{\nu})^{-4} \tilde{\nu} [n(\tilde{\nu}, T) + 1]^{-1} I^{\text{exp}}(\tilde{\nu}), \quad (1)$$

where  $n(\tilde{\nu}, T) = [\exp(\hbar\tilde{\nu}/k_B T) - 1]^{-1}$  is the Bose occupation number ( $\hbar$  and  $k_B$  are the Planck and Boltzmann constants, respectively); the term in the fourth power is the correction for the wavelength dependence of the scattered intensity;  $\tilde{\nu}$  is the Raman shift in  $\text{cm}^{-1}$ , and  $\tilde{\nu}_0$  denotes the wavenumber of the incident radiation. Reduction of the Raman spectra is further needed in order to compare experimental and theoretical vibrational modes. Indeed, using the vibrational frequencies and the Raman activities obtained by *ab initio* calculations, a theoretical spectrum can be constructed and compared with the reduced experimental spectrum.

Fig. 1 illustrates the as-recorded and the reduced Raman spectra of selected  $(\text{AgI})_x(\text{AsSe})_{100-x}$  glasses. The spectra have been normalized (arbitrarily) in order to highlight the changes in the relative peak intensities. It is evidently shown that the reduction procedure severely alters the relative intensities of the Raman bands, which has a strong impact on the quantitative analysis in terms of structural units. The Raman spectra reveal that appreciable structural changes take place upon alloying the ChG with AgI. The spectrum of the AsSe glass exhibits a few sharp peaks superimposed on a broad background at high energies, in the range  $180\text{--}300 \text{ cm}^{-1}$ , which are assigned (see below) to bond stretching vibrational modes and a number of sharper ones at low frequencies [ $110\text{--}175 \text{ cm}^{-1}$ ] originating from bond bending or deformation modes of the various structural units. The addition of AgI causes severe reduction in the intensity of the sharp high energy peaks at 221, 237, and  $247 \text{ cm}^{-1}$ , which become severely suppressed for AgI 30%, while a new sharp mode appears at  $213 \text{ cm}^{-1}$ . In the bending mode regime, relative intensity changes are mainly observed, while the number of these sharp modes does not depend on the AgI content. The overall spectral envelope from 200 to  $300 \text{ cm}^{-1}$  narrows progressively with AgI addition.

The aforementioned changes contrast markedly the behavior of AgI-doped  $\text{Ge}_2\text{S}_3$  glasses [11]. The structure of  $\text{Ge}_2\text{S}_3$  glass is network-like where heteronuclear Ge–S and homonuclear Ge–Ge types of bonds can be found. Specifically, the structure of the  $\text{Ge}_2\text{S}_3$  glass was described by an interconnection of mixed tetrahedra of the form  $\text{Ge}_n\text{Ge}_{4-n}$  ( $n=0, 1, 2, 3, 4$ ) [11]. It is interesting to note that although both glass matrices, AsSe and  $\text{Ge}_2\text{S}_3$ , are at the overstoichiometric regime, the addition of AgI causes effectively more drastic structural modifications in the case of the AsSe glass as revealed by the significant spectral changes in Raman spectra. On the contrary, the addition of AgI causes mild changes in the structure of the  $\text{Ge}_2\text{S}_3$  glass pointing to a non-network-modifier role of the AgI additive [11]. The origin of the contrasting behavior between the two modified glasses is partly associated with the enhanced molecular-like nature of the AsSe glass in comparison with the  $\text{Ge}_2\text{S}_3$  glass; see next section for details.

The Raman spectra shown in Fig. 1 reveal that in order to describe the structure of the AsSe glass a network-like component of mixed pyramidal units  $\text{As–As}_3\text{–}_n\text{Se}_n$  [12,13] as well as a

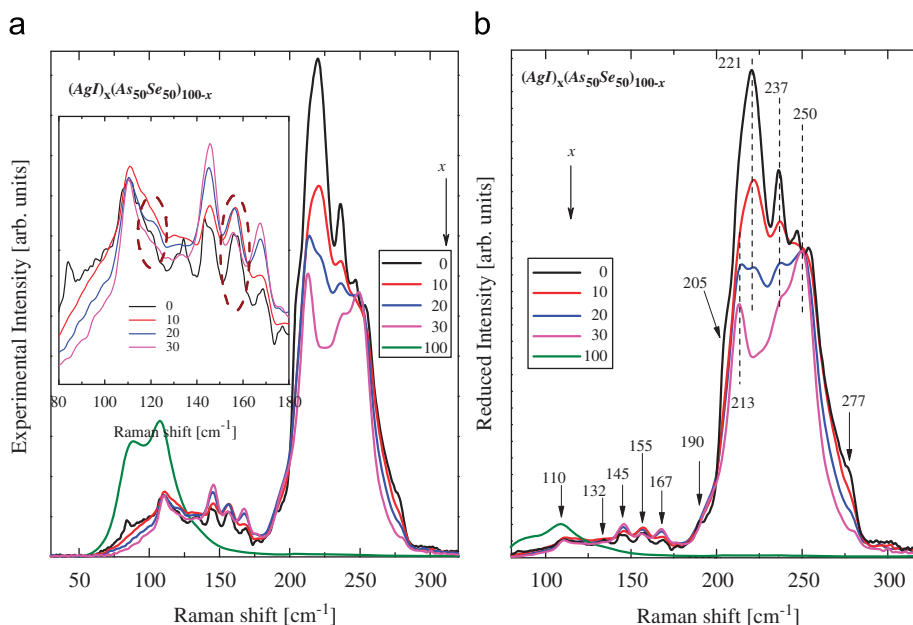


**Fig. 1.** (a) Experimental and (b) reduced Raman spectra of  $(\text{AgI})_x(\text{As}_{50}\text{Se}_{50})_{100-x}$  glasses and crystalline AgI. (a) A magnification of the low energy spectral region. Raman bands related to amorphous As (see Section 4.1 for details) are encircled in dashed lines.

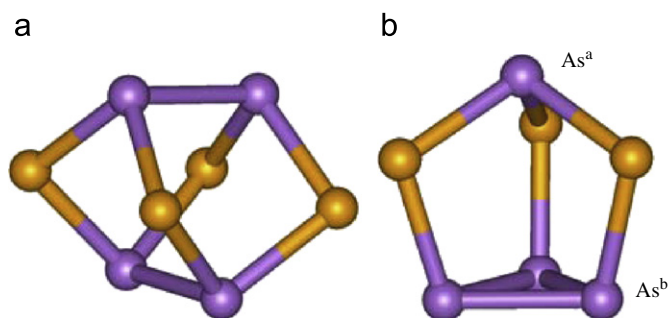


**Fig. 2.** Ball and stick draws of the HF fully optimized structures of highly symmetric  $\text{As}_4\text{S}_m$  (a)  $m=4$ , and (b)  $m=3$  cage-like structural models. Purple and dark yellow atoms represent As and Se, respectively.  $\text{As}^a$  and  $\text{As}^b$  stand for apical and basal As atoms in  $\text{As}_4\text{Se}_3$ . (For interpretation of the references to color in this figure legend, the reader is referred to the web version of this article.)

number of discrete cage-like molecules must be invoked. Due to the proximity of the masses of As and Se atoms, their vibrational modes are situated at the same energy range and thus the interpretation of the Raman spectra of As–Se glasses, especially in the As-rich regime, is very complicated. On the other hand, the molecular cage-like units  $\text{As}_4\text{Se}_m$  ( $m=3$  or 4) exhibit much sharper Raman peaks in comparison with network-like structures and the peak identification is more straightforward.

Using the first principles methods described in Section 2.2 we have undertaken a fully optimization of the structures of the cage-like molecules shown in Fig. 2. In  $\text{As}_4\text{Se}_4$  ( $D_{2d}$  symmetry, realgar-type molecule) there are two homonuclear As–As bonds; all As atoms are equivalent. On the other hand, in  $\text{As}_4\text{Se}_3$  ( $C_{3v}$  symmetry) there are three equivalent As atoms forming the basal triangle of the unit and an apex As atom which is bonded to three Se atoms. Table 1 contains the structural parameters of the cage-like units as estimated by the HF/TZV method.  $\text{As}^b$  and  $\text{As}^a$  stand for the basal and apical As atoms, respectively, in  $\text{As}_4\text{Se}_3$ . Our structural data are in very good agreement with the corresponding experimental values [14,15]. *Ab initio* calculations for  $\text{As}_4\text{Se}_4$  have also been performed [16]; however, no geometrical details were reported. For the  $\text{As}_4\text{Se}_3$  molecule, no such experimental or

**Table 1**

Calculated and experimental bond distances ( $\text{\AA}$ ) and angles ( $^\circ$ ) at the HF/TZV level of the theory, for the  $\text{As}_4\text{Se}_4$  and  $\text{As}_4\text{Se}_3$  cage-like models with  $D_{2d}$  and  $C_{3v}$  symmetry, respectively.

Bond length/angle	$\text{As}_4\text{Se}_4$ ( $D_{2d}$ )		$\text{As}_4\text{Se}_3$ ( $C_{3v}$ )
	HF/TZV	Exp. <sup>a,b</sup>	HF/TZV
$R(\text{As}-\text{As})$	2.555	2.564, 2.565	2.461
$R(\text{As}-\text{Se})$	2.377	2.388, 2.39	( $\text{As}^a-\text{Se}$ ) 2.371 ( $\text{As}^b-\text{Se}$ ) 2.367
$\angle(\text{As}-\text{Se}-\text{As})$	97.6	98.1, 97.2	101.9
$\angle(\text{Se}-\text{As}-\text{Se})$	94.6	94.1, 94.7	99.4
$\angle(\text{As}-\text{As}-\text{Se})$	101.4	101.2, 101.5	104.1

<sup>a</sup> Taken from Ref. [14].

<sup>b</sup> Taken from Ref. [15].

**Table 2**

Calculated and scaled Raman and IR harmonic frequencies ( $\text{cm}^{-1}$ ) at HF/TZV level of theory and experimental Raman frequencies of the  $\text{As}_4\text{Se}_4$  cage-like model ( $D_{2d}$  symmetry). The brackets contain the calculated intensities in the following form [Raman activity in  $\text{\AA}^4 \cdot (\text{amu})^{-1}/\text{depolarization ratio}$ , IR intensity in  $\text{km mol}^{-1}$ ]. Intensities and activities less than 0.1 have been set equal to zero.

No	Symmetry	HF/TZV calculated	HF/TZV scaled	Experimental <sup>a</sup>
1	$A_2$	75.3 [0/0.41,0]	64.0	Inactive
2	$E$	125.1 [1/0.75,0.9]	106.3	
3	$B_1$	130.0 [8.5/0.75,0]	110.5	152 ( $\delta$ As–Se–As)
4	$B_2$	151.4 [4.6/0.75,1.3]	128.7	
5	$A_1$	171.1 [14/0.33,0]	145.4	144 ( $\delta$ As–Se–As)
6	$E$	202.6 [4/0.75,0.2]	172.2	
7	$B_2$	222.0 [3.9/0.75,1.9]	188.7	190 ( $\nu$ As–As)
8	$A_1$	239.7 [25.2/0,0]	203.7	207 ( $\nu$ As–As)
9	$A_2$	279.9 [0/0.67,0]	237.9	
10	$E$	282.7 [5/0.75,13]	240.3	
11	$B_2$	285.3 [2.9/0.75,10.7]	242.5	240 ( $\nu$ As–Se) <sup>b</sup>
12	$E$	287.2 [0/0.75,0.3]	244.1	
13	$B_1$	290.4 [6/0.75,0]	246.8	235 ( $\nu$ As–Se)
14	$A_1$	290.6 [23.6/0,0]	247.0	248 ( $\nu$ As–Se)

<sup>a</sup> Taken from Ref. [17].

<sup>b</sup> IR frequency.

theoretical structural analysis has been reported so far in the literature.

Vibrational analysis was performed at the HF level theory for both molecules in order to obtain the harmonic frequencies of their vibrational modes. A complete list of the harmonic frequencies of both molecules together with the assignment of these modes is compiled in Tables 2 and 3 for  $As_4Se_4$  and  $As_4Se_3$ , respectively, in comparison with previous experimental data [17,18]. The tables contain the harmonic frequencies of Raman and infrared active modes and the corresponding Raman activities. It is common that calculated frequencies of isolated molecules differ from the true experimental values if these molecules are embedded in a condensed phase due to the effect of environment (intermolecular interactions). This discrepancy does not exist when comparing calculated and experimental data of molecules in the gaseous phase. Further sources of disagreement between theoretical and experimental frequencies are the neglect of anharmonicity in theoretical calculations, the incomplete incorporation of electron correlation, and the use of finite basis sets. Therefore, in order to correctly compare experimental and calculated spectra, scaling factors are frequently employed. Fig. 3

**Table 3**

Calculated and scaled Raman and IR harmonic wavenumbers ( $cm^{-1}$ ) at HF/TZV level of theory and experimental Raman frequencies of the  $As_4Se_3$  cage-like model ( $C_{3v}$  symmetry). The brackets contain the calculated intensities in the following form [Raman activity in  $\text{\AA}^4 \cdot (\text{amu})^{-1}$ /depolarization ratio, IR intensity in  $\text{km mol}^{-1}$ ]. Intensities and activities less than 0.1 have been set equal to zero.

No	Symmetry	HF/TZV calculated	HF/TZV scaled	Experimental <sup>1</sup>
1	$A_2$	104.9 [0/0.75,0]	91.3	
2	$E$	121.2 [2.8/0.75,1.2]	105.4	109 ( $\delta$ $As^a-Se_3$ )
3	$E$	169.3 [8.1/0.75,0]	147.3	144 ( $\delta$ $As^b-Se$ )
4	$A_1$	199.7 [7.1/0.57,0.1]	173.7	166 ( $\delta$ $As^a-Se_3$ )
5	$E$	224.4 [8.8/0.75,1.1]	195.2	199 ( $\nu$ $As_3$ )
6	$A_1$	266.9 [42/0.01,1.5]	232.2	233 ( $\nu$ $As^a-Se_3$ )
7	$A_1$	280.0 [0.7/0.30,11.8]	243.6	243 ( $\nu$ $As^b-Se$ )
8	$E$	286.7 [3.0/0.75,7.0]	249.4	236 ( $\nu$ $As^b-Se$ )
9	$E$	299.1 [0/0.75,0.1]	260.2	263 ( $\nu$ $As^a-Se_3$ )
10	$A_1$	326.4 [11.4/0.15,0.2]	283.9	278 ( $\nu$ $As_3$ )

<sup>1</sup> Taken from Ref. [18].

shows experimental and theoretical Raman spectra for the  $As_4Se_4$  and  $As_4Se_3$  cage molecules. The experimental Raman spectra for  $As_4Se_4$  and  $As_4Se_3$  are taken from Refs. [18,19], respectively. Calculated spectra are constructed from the harmonic vibrational frequencies and Raman activities obtained using Gaussian type distributions. A common full width of  $5\text{ cm}^{-1}$  was chosen for all vibrational lines to achieve a satisfactory agreement in the spectral shape of experimental and calculated curves.

The theoretical spectra were scaled by a common factor for all Raman modes. The scaling factor for  $As_4Se_4$  is 0.85 and corresponds to the factor needed to bring into coincidence the symmetric stretching As–Se vibrational mode, which is calculated at  $291\text{ cm}^{-1}$  (experimental value  $248\text{ cm}^{-1}$ ). We observe that with a single scaling factor we achieve a very good agreement between experimental and calculated spectra. The theoretical frequency of the symmetric stretching As–As vibrational mode (scaled value:  $204\text{ cm}^{-1}$ ) and its relative intensity is very close to the experimental value ( $207\text{ cm}^{-1}$ ). The calculated values for band positions and relative intensities are less accurate for bending and deformation modes. However, the agreement can be considered satisfactory, considering the neglect of intermolecular interactions in the *ab initio* calculations. The scaling factor of  $As_4Se_3$  (0.87) also results in a satisfactory agreement between experiment and calculations. In this case the matching was performed at the vibrational mode, which describes the symmetric breathing mode of the whole molecule, located at  $233\text{ cm}^{-1}$ . The scaling factors emerged in this work are within the typical range [21] for *ab initio* simulations performed with the HF method.

## 4. Discussion

### 4.1. Structure of glassy AsSe

It is worth mentioning that more details are known about photoinduced effects (see for example optomechanical [8] and photoplastic [22] effects) exhibited by the AsSe glass than about its short- and medium-range structural order. It is known that the structure of As–Se glasses is strongly dependent on the glass stoichiometry. In Se-rich glasses, long helical Se chains and  $AsSe_{3/2}$  pyramidal units are the main structural building blocks. The addition of As results in the formation of a network-like

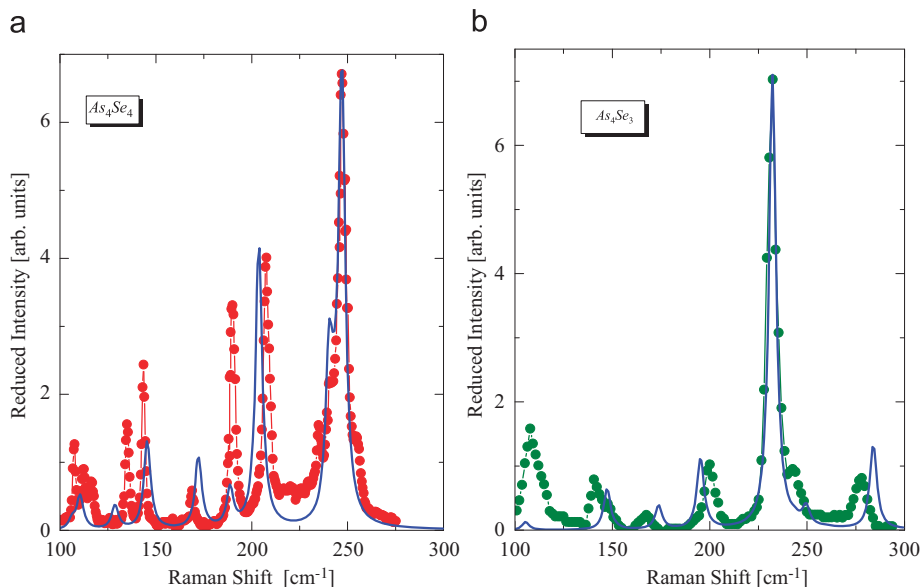


**Fig. 3.** Experimental (solid circles) and theoretically calculated (solid lines) Raman spectra of crystalline (a)  $As_4Se_4$  and (b)  $As_4Se_3$ ; see text for details.



structure of low dimensionality [4]. This process continues up to an As content of 40% where two-dimensional layers of  $\text{AsSe}_{3/2}$  corner-sharing pyramids in few-member rings form. At this point many physical properties of the binary system, such as glass transition temperature,  $T_g$ , and the shear modulus, are maximized [4]. Interesting effects occur upon a further increase of As atoms where molecular species start forming. At the equimolar composition,  $x=50$ , besides the glass, there exists a stable crystalline form with the realgar structure of the corresponding arsenic sulfide compound. Structural studies using X-ray photoelectron spectroscopy (XPS) of  $\text{As}_x\text{Se}_{100-x}$  films with  $x > 40$  have been interpreted to be compatible with mixed pyramidal units of the form  $\text{As}-\text{As}_{3-n}\text{Se}_n$  ( $n=0, 1, 2, 3$ ) [12,13]. However, the existence of molecular-like species as  $\text{As}_4\text{Se}_m$  ( $m=4$  or  $3$ ) could not be ruled out or confirmed by analyzing XPS data. The decrease of  $T_g$  in comparison with the maximum value at the stoichiometric composition [4] implies a rather gentle network modification by the presence of extra As atoms.

The structure of As-rich, As–Se glasses has been studied by diffraction methods [23] pointing to the suggestion that that pyramidal  $\text{AsSe}_{3/2}$  and cage-like  $\text{As}_4\text{Se}_4$  structural units exist in bulk glasses. Leadbetter and Apling [24] studied  $\text{As}_x\text{Se}_{100-x}$  glasses ( $30 \leq x \leq 50$ ) by X-ray and neutron diffraction interpreting their data as being consistent with a layered structure and the satisfaction of the 8-N rule for coordination of As and Se. In an EXAFS study, Elliott and Kolobov [25] compared the structure of an a- $\text{As}_{50}\text{Se}_{50}$  film and the corresponding bulk glass. They reported that there are not significant changes in the short-range order. Arsenic is coordinated on the average by 2.4 Se atoms and by 0.7 As atoms. Selenium is coordinated by 1.8 As atoms. A detailed EXAFS study for binary glasses  $\text{As}_x\text{Se}_{100-x}$  glasses ( $20 \leq x \leq 57$ ) have been undertaken by Mastelaro et al. [26]. The analysis revealed the existence of homonuclear As–As bonds in the As-rich region. Infrared reflectance spectra have also been used and provided some details about the structure of As-rich glasses [27,28] suggesting the existence of particular structural units in the Se-rich and As-rich composition domains. Finally, structural details about As–Se glasses have also been inferred by analyzing temperature-modulated differential scanning calorimetry results [29,30]. In the most recent study [31], the atomic structure of the  $\text{As}_{50}\text{Se}_{50}$  was studied by X-ray, neutron diffraction, and EXAFS, modeling all experimental data simultaneously by the reverse Monte Carlo technique. The analysis was consistent with coordination numbers  $N_{\text{As}-\text{As}}=1.03 \pm 0.05$  and  $N_{\text{As}-\text{Se}}=1.97 \pm 0.08$ .

Given the above brief literature survey on the structure of vitreous  $\text{As}_{50}\text{Se}_{50}$ , it becomes obvious the necessity of Raman scattering, a species-specific technique, to analyze in detail the structure of this glass and its change upon alloying with AgI. The elucidation of the vibrational properties of the most possible cage-like molecules will augment this attempt. To facilitate the discussion, we compare in Fig. 4 the experimental reduced Raman spectra of the AgI-free glasses AsSe and  $\text{As}_2\text{Se}_3$  together with the Raman spectra derived from *ab initio* calculations. The network-like nature of the stoichiometric glass structure, dominated by corner-sharing  $\text{AsSe}_{3/2}$  pyramids, is characteristically reflected by the very broad, featureless Raman spectrum in the spectral range 200–300  $\text{cm}^{-1}$ . The addition of extra As atoms, over the stoichiometric threshold, causes partial network degradation as evidenced from the appearance of sharp peaks in the spectrum of the AsSe glass, which are, however, superimposed on a remaining broader spectrum.

The decomposition of the Raman spectrum of the AsSe glass into its individual vibrational lines, using Gaussian type distributions, is shown in Fig. 5(a). The breadth of the spectrum renders the interpretation of the various lines complicated. The reason is

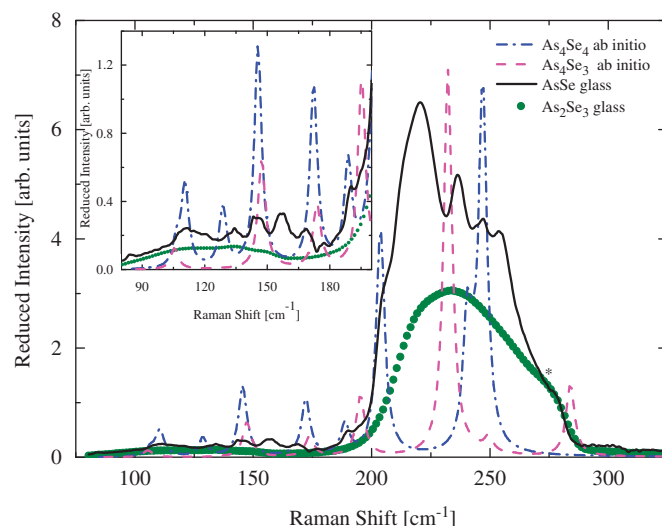


**Fig. 4.** Experimental Raman spectra of glassy AsSe and  $\text{As}_2\text{Se}_3$ . The theoretically calculated Raman spectra of  $\text{As}_4\text{Se}_4$  and  $\text{As}_4\text{Se}_3$  have been added for comparison. The inset shows the low energy region in magnification.

that the structure of the AsSe glass can be considered as a combination of three sub-structures:

- I. a stoichiometric-like one, resembling the structure of  $\text{As}_2\text{Se}_3$ , composed of corner-sharing  $\text{AsSe}_{3/2}$  pyramids;
- II. a contribution from mixed pyramids  $\text{As}-\text{As}_{3-n}\text{Se}_n$ , ( $n=0, 1, 2,$ ); and
- III. a fraction of cage-like molecules ( $\text{As}_4\text{Se}_4$ ,  $\text{As}_4\text{Se}_3$ ) decoupled from the network structure.

Sub-structures of type II and III will be called henceforth the As-rich components. Within the above context, we can adopt a simpler approach to clarify the structural features of the AsSe glass. In a first approximation, we can estimate the Raman spectrum that corresponds to the As-rich sub-structures as the difference between the Raman spectra of the stoichiometric and the AsSe glasses, after proper scaling. As shown in Fig. 4, we have chosen to scale the two spectra at the region of  $\sim 275 \text{ cm}^{-1}$  (marked by a star) due to the existence in this spectral range of a characteristic line of network-like origin, which exists in both spectra. The difference spectrum, which apparently represents the vibrational lines originating from the As-rich structural species present in the AsSe glass, is illustrated in Fig. 5(b). It is analyzed with a sum of Gaussian distribution peaks whose energy positions are shown in the figure. Absolute errors for band frequencies, as provided by the analysis, are less than  $0.5 \text{ cm}^{-1}$  apart from the not well-resolved lines at  $195.8$  and  $260.9 \text{ cm}^{-1}$  where the errors amount to  $\sim 1.0 \text{ cm}^{-1}$ . Following the analysis described above the interpretation of the new modes becomes more straightforward. The bands at  $189.5$  and  $195.8 \text{ cm}^{-1}$  are assigned to anti-symmetric stretching frequencies of  $\nu(\text{As}-\text{As})$  and  $\nu(\text{As}_3^3)$  in the  $\text{As}_4\text{Se}_4$  and  $\text{As}_4\text{Se}_3$  molecules, respectively. The sharp mode at  $236.8 \text{ cm}^{-1}$  is near the symmetric stretching mode of the  $\text{As}^2\text{Se}_3$  pyramid of  $\text{As}_4\text{Se}_3$  located at  $233 \text{ cm}^{-1}$ ; a slight shift of about  $4 \text{ cm}^{-1}$  can be accounted for by the different degree of intermolecular interactions, which these cage-like molecules experience in the crystalline and in the glassy phase. Further, the  $247.3 \text{ cm}^{-1}$  mode is assigned to the  $\nu(\text{As}-\text{Se})$  symmetric stretching mode of  $\text{As}_4\text{Se}_4$  molecules (see Fig. 4).

The intense spectral envelope  $200\text{--}240 \text{ cm}^{-1}$  (exhibiting its maximum at  $220 \text{ cm}^{-1}$ ) and the weaker bands at  $156$  and  $120 \text{ cm}^{-1}$  are signatures of vibrations of elemental amorphous

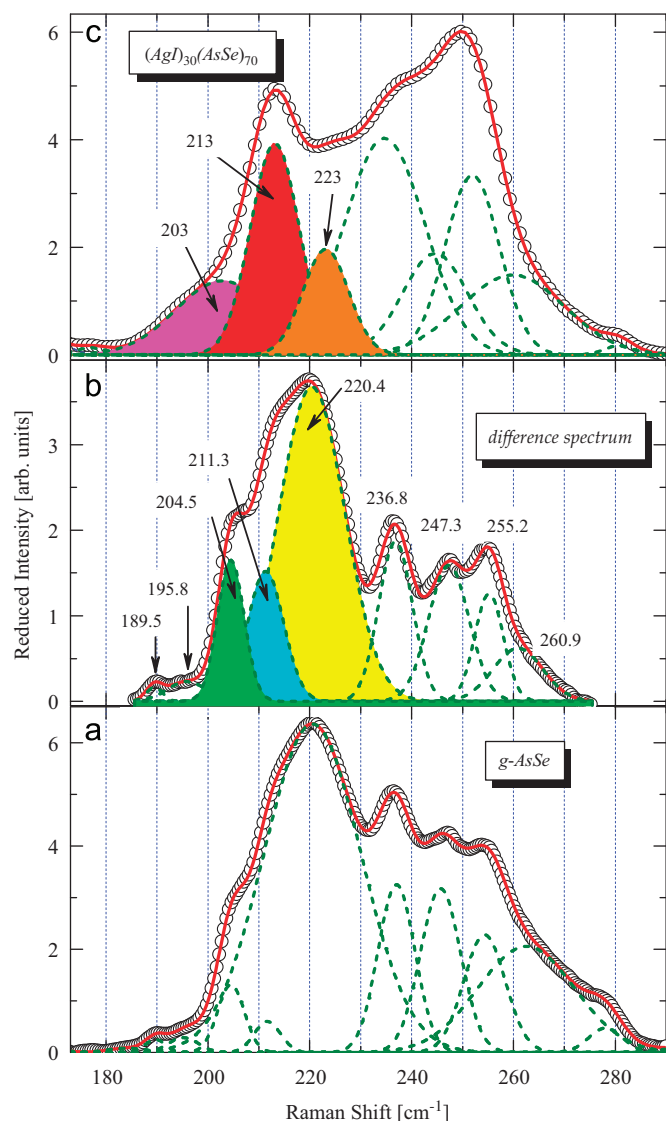


**Fig. 5.** (a) Difference spectrum between of the reduced Raman spectra of glassy  $\text{AgI}_{30}(\text{As}_{50}\text{Se}_{50})_{70}$  and  $\text{As}_2\text{Se}_3$ . (b) Reduced Raman spectrum of glassy  $\text{As}_{50}\text{Se}_{50}$ . (c) Reduced Raman spectrum of  $\text{AgI}_{30}(\text{As}_{50}\text{Se}_{50})_{70}$ . Open circles: experimental data points (only 50% of data points are shown for clarity). The thick solid line through the data points is the best fit result. Dashed lines represent the Gaussian distribution for the individual vibrational modes.

As [32] or As-rich domains. Indeed, these bands exhibit a common trend, i.e. become systematically weaker with the increase of AgI as seen in Fig. 1(a) and its inset. The spectral envelope 200–240  $\text{cm}^{-1}$  is decomposed into three bands situated at 204.5, 211.3, and 220.4  $\text{cm}^{-1}$ . We suggest that these bands are possibly associated with the stretching vibrational modes of As–As bonds in As-rich ( $n=0, 1$ ) mixed pyramids  $\text{As}-\text{As}_{3-n}\text{Se}_n$ . Finally, the two peaks at higher energies, 255.2, 260.9  $\text{cm}^{-1}$ , are possibly associated with vibrational modes of the mixed pyramids  $\text{As}-\text{As}_{3-n}\text{Se}_n$  that appear due to the removal of degeneracy in the reduction of the  $C_{3v}$  symmetry for pyramids with  $n=3$  to  $C_s$  symmetry for pyramids with  $n=1, 2$ .

#### 4.2. AgI-induced structural changes in glassy AsSe

As shown in Fig. 1, the addition of AgI causes severe changes in the structure of the AsSe glass. This finding has to be compared with the structural changes in other similar glasses  $(\text{AgI})_x(\text{As}_2\text{Se}_3)_{100-x}$  [33] where it was reported that the Raman spectra

of the mixtures for AgI contents up to 60 mol% are almost identical with that of the  $\text{As}_2\text{Se}_3$  glass. To account for this observation, it was suggested [33] that the network matrix in the mixed glasses consists of  $\text{AsSe}_{3/2}$  pyramidal units, whilst a significant number of Ag atoms are tetrahedrally bonded to I, in a similar way as in crystalline  $\alpha$ -AgI. In that sense, the structure for these glasses is considered to be phase separated in a stoichiometric-like ( $\text{As}_2\text{Se}_3$ ) backbone and dispersed AgI clusters. Comparing the Raman spectra of the AgI-doped  $\text{As}_2\text{Se}_3$  glass [33] and the AgI-doped AsSe glass in our case we conclude that the existence of homonuclear As–As bonds ( $E^{\text{bond}}=46$  kcal/mol) act as the weak centers, which are more easily disrupted by iodine ions than As–Se bonds ( $E^{\text{bond}}=52$  kcal/mol). Moreover, the difference in Pauli electronegativities between the As, I and As, Se pairs is  $\sim 30\%$  higher in the former providing further justification to the preference of I atoms to bond to As ones.

Inspecting Fig. 1 it becomes evident that iodine ions attack As–As bonds in both As-rich sub-structures described in Section 4.1. Indeed, we observe decrease in the intensity of the sharp lines at 221, 237, and 247  $\text{cm}^{-1}$ , which eventually disappear for AgI 30%. The first arises from As-rich environments in mixed pyramids, while the other two originate from vibrations of the decoupled cage-like molecules ( $\text{As}_4\text{Se}_4$ ,  $\text{As}_4\text{Se}_3$ ). Further, it is evident the decrease in the breadth of the spectral envelope 200–280  $\text{cm}^{-1}$ , which reflects depletion of network modes of the sub-structure composed of mixed pyramids  $\text{As}-\text{As}_{3-n}\text{Se}_n$ . In addition, the degradation of the mixed pyramidal network, due to AgI addition, is further implied by the systematic decrease of the band at 277  $\text{cm}^{-1}$  and of the low-frequency background below 100  $\text{cm}^{-1}$ .

To better understand the nature of structural changes brought about by AgI one should be able to elucidate the individual role of Ag and I ions. Some information has been provided by recent X-ray and neutron diffraction studies where the structural function of each atom, Ag and I, to AsSe glass was studied separately [31]. It was suggested that Ag tends to form bonds with Se atoms increasing the connectivity of the glass structure. On the contrary, iodine bonds preferentially to As atoms causing the reduction in the mean coordination number and the network structure of the glass. We therefore expect, in the present case, that the addition of both ions Ag and I simultaneously will cause complementary structural modifications. The newly formed Ag–Se bonds are of ionic character with small Raman cross section, and the corresponding vibrational modes are therefore expected rather diffuse and broad in the Raman spectra. The Ag–Se vibrational frequency lies at an energy range near 200  $\text{cm}^{-1}$  [34]. On the other hand, the newly formed As–I (terminal) bonds exist in mixed chalcogenide pyramids  $\text{AsSe}_m\text{I}_{3-m}$  ( $m=0, 1, 2$ ) and will appear more intense and sharper in the Raman spectrum owing to the high polarizability of the As–I bond and the well defined geometry of the pyramids, respectively.

In order to identify the Raman bands of these new species we have to recall that the  $\text{AsI}_3$  pyramidal unit ( $C_{3v}$  symmetry) exhibits its symmetric  $\nu_1(A)$  and anti-symmetric  $\nu_3(E)$  stretching vibrational modes at 212 and 201  $\text{cm}^{-1}$ , respectively, in the gaseous phase [35] and at 216 and 221  $\text{cm}^{-1}$ , respectively, in solutions [36], where intermolecular interactions are stronger. Bending modes are weak and located below 90  $\text{cm}^{-1}$ , thus not resolved in the present study. We observe that the anti-symmetric mode frequency is significantly affected by the environment, being higher than the symmetric one when intermolecular interactions are stronger; a fact related probably to the change of the apex angle of the trigonal pyramid. Using a Gaussian line fitting we have decomposed the spectrum of the more heavily doped glass, i.e.  $(\text{AgI})_{30}(\text{As}_{50}\text{Se}_{50})_{70}$ , into its vibrational lines as illustrated in Fig. 5(c). It is instructive to compare this analysis with that we have followed for the difference spectrum in

**Table 4**

Bond lengths, unscaled harmonic vibrational frequencies (Raman), and atomic charges calculated at HF/DZVP level of theory for the pyramidal units shown. Numbers in parentheses stand for the Raman activity of the modes given in  $\text{\AA}^4 \cdot (\text{amu})^{-1}$  units. The first row shows HF fully optimized ball-and-stick draws of the pyramidal units. Purple: As; Dark yellow: Se; Red: I; Light gray: H.

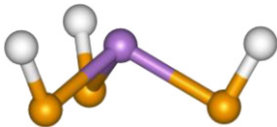
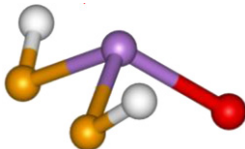
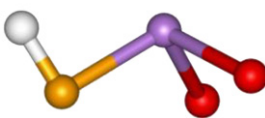
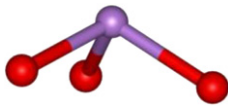
Model				
Symmetry	$C_{3v}$	$C_s$	$C_s$	$C_{3v}$
$r(\text{As-Se})$ (Å)	2.398	2.385	2.388	–
$r(\text{As-I})$ (Å)	–	2.624	2.594	2.588
$\nu^{\text{ss}}(\text{As-Se})$ ( $\text{cm}^{-1}$ )	270.1 (38.0)	290.1 (24.2)	292.3 (18.2)	–
$\nu^{\text{ss}}(\text{As-I})$ ( $\text{cm}^{-1}$ )	–	232.9 (23.4)	239.2 (28.0)	236.6 (27.2)
$\nu^{\text{as}}(\text{As-Se})$ ( $\text{cm}^{-1}$ )	297.0 (15.7)	298.1 (13.0)	–	–
$\nu^{\text{ss}}(\text{As-I})$ ( $\text{cm}^{-1}$ )	–	–	249.8 (15.7)	251.3 (15.1)
$q$ (As/Se/I)	0.25/–0.25/–	0.31/–0.22/–0.21	0.32/–0.20/–0.14	0.36/–/–0.12

Fig. 5(b), which represents vibrations of As-rich sub-structures of type II and III. Upon adding AgI: (a) we observe a severe depletion of the main bands of the type II sub-structure, i.e.  $\text{As-As}_{3-n}\text{Se}_n$  pyramids, at 204.5, 211.3, and  $220.4 \text{ cm}^{-1}$ , which are almost absent in the spectrum of the AgI 30% glass; (b) the 236.8, 247.3, and  $255.2 \text{ cm}^{-1}$  are practically not resolved in the AgI-doped glass.

Before proceeding to the assignment of the various lines composing the Raman spectrum of the Ag 30% glass we have to take into account that two types of As–I bonding exist, i.e. As–I bonds in pure halide pyramids  $\text{AsI}_3$  ( $m=0$ ) and As–I bonds in mixed chalcogenide pyramids  $\text{AsSe}_2\text{I}$ ,  $\text{AsSe}_2\text{I}$  ( $m=1, 2$ ). The different electronic structure of As atoms in neat (halide) and mixed (chalcogenide) pyramids has an impact in the As–I bonding. Using the methods described in Section 2.2 we have calculated the structure and harmonic frequencies of all possible combinations of  $\text{AsSe}_m\text{I}_{3-m}$  pyramids. Se atoms are terminated by H atoms as shown in the ball-and-stick draws in Table 4. The table also contains the unscaled (symmetric stretching  $\nu^{\text{ss}}$  and anti-symmetric stretching  $\nu^{\text{as}}$ ), harmonic vibrational frequencies of the neat  $\text{AsSe}_3$ ,  $\text{AsI}_3$  and the mixed  $\text{AsSe}_2\text{I}$ ,  $\text{AsSe}_2\text{I}$  pyramids. The As–Se bond, in mixed pyramids, strengthens in comparison with its value in the neat  $\text{AsSe}_3$  pyramid. The corresponding As–Se vibrational frequencies shift to higher values in mixed chalcogenide pyramids. Similar trend in As–Se bond length was observed in diffraction studies [31]. On the contrary, the As–I bond seems to become longer (weaker) only in the iodine-poor pyramid  $\text{AsSe}_2\text{I}$ . This result is supported by the appreciable increase of the I atom charge as compared to the charges of the iodine-rich pyramids. The stretching vibrational frequency of the As–I terminal bonds seems not particularly dependent on the type of pyramid into which is embedded. A factor of 0.896 is needed to scale experimental (gas phase) and theoretical frequencies for  $\text{AsI}_3$ . The corresponding factor for  $\text{As}_2\text{I}_3$  is 0.866; however, in this case the comparison of the calculated value is done with the glass phase where intermolecular interactions are responsible for the higher deviation. As in the case of the  $\text{As}_4\text{Se}_m$  molecules, the scaling factors of the pyramidal units lie with the typical range for *ab initio* HF calculations [21].

Based on this information, we consider the following assignments for the decomposed Raman lines of the  $(\text{AgI})_{30}(\text{As}_{50}\text{Se}_{50})_{70}$  glass. The line at  $213 \text{ cm}^{-1}$  is associated with the bond stretching frequency of the As–I bonds in any type of pyramids. The  $223 \text{ cm}^{-1}$  peak is attributed to the anti-symmetric bond

stretching vibrational mode of the As–I bond in  $\text{AsI}_3$  and  $\text{AsSe}_2\text{I}$ , pyramids. The experimental ratio  $(\nu^{\text{as}}/\nu^{\text{ss}})^{\text{expt}}=1.047$  is in very good agreement with the calculated one  $(\nu^{\text{as}}/\nu^{\text{ss}})^{\text{cal}}=1.062$  and 1.044 for  $\text{AsI}_3$  and  $\text{AsSe}_2\text{I}$ , respectively. The origin of the broad peak centered at  $\sim 203 \text{ cm}^{-1}$  is not so clear. As stated above, the Ag–Se vibrational mode is expected to near or below  $200 \text{ cm}^{-1}$  [34]. In addition, the lift of degeneracy owing to the symmetry reduction from  $C_{3v}$  in neat pyramids to  $C_s$  in mixed chalcogenide pyramids (see Table 4) has as a consequence the appearance of new Raman active modes. Therefore, the band at  $\sim 203 \text{ cm}^{-1}$  is possible associated with overlapping lines of Ag–Se and As–I vibrational modes.

The analyzed spectrum of the  $(\text{AgI})_{30}(\text{AsSe})_{70}$  glass contains also intense peaks at 235, 245, 252, and  $260 \text{ cm}^{-1}$ . Based on the finding that the As–Se bonds strengthens in the mixed chalcogenide glass in comparison with the pure AsSe glass, these bands can be assigned to vibrational modes of the network of corner-sharing  $\text{AsSe}_{3/2}$  pyramids (sub-structure of type I). The calculated blue-shift of the As–Se vibrational frequencies is of about 8%; thus the characteristic (experimental) frequency of corner-sharing  $\text{AsSe}_{3/2}$  pyramids at  $230 \text{ cm}^{-1}$  is expected to shift to  $\sim 250 \text{ cm}^{-1}$  in AgI-doped glasses. However, the presence of some As-rich fragments either of type II or III cannot be excluded in view of the experimental (diffraction) data which show that a non-negligible fraction of As–As bonds exists in the structure of the glass with 35% AgI [31]. Indeed, as shown in the inset of Fig. 1, the bending modes of the cage-like units exhibit a peculiar behavior as function of AgI content. In particular, while the stretching modes of the cage-like units at high energies seem to disappear with increasing AgI in the glass, the opposite occurs for their bending modes. A possible rationale of this odd trend could adopt a drastic relative change in the Raman cross section of bending and stretching modes of the cage-like units upon the variation of their immediate environment when alloying the  $\text{As}_{50}\text{Se}_{50}$  glass with AgI.

## 5. Conclusions

Raman scattering and *ab initio* calculations have been employed to study structural details of AgI-doped AsSe glasses. Calculations were applied to cage-like molecular  $\text{As}_n\text{Se}_n$  ( $n=3, 4$ ) units, providing geometrical data (bond lengths and angles) and harmonic vibrational frequencies. The calculated Raman spectra

exhibit satisfactory agreement with the experimental ones for the corresponding molecular crystals. Analysis of reduced Raman spectra revealed that the  $As_{50}Se_{50}$  glass structure can be described by three sub-structures, i.e. a network of corner-sharing  $As_2Se_3$  pyramids, a network of mixed  $As-As_{3-n}Se_n$  pyramids, and molecules ( $As_4Se_4$ ,  $As_4Se_3$ ) decoupled from the network structure. The addition of AgI causes appreciable structural changes and in particular the reduction of the As-rich environments, i.e. mixed pyramids and cage-like molecules. Assignments of the vibrational modes in heavily doped AgI glasses have been assisted by *ab initio* calculations of the harmonic frequencies of neat  $AsSe_3$ ,  $AsI_3$ , and mixed  $AsSeI_2$ ,  $AsSe_2I$  pyramids.

## References

- [1] For a collection of photoinduced effects in ChGs see: A.V. Kolobov, (Ed.), Photo-induced Metastability in Amorphous Semiconductors, Wiley-VCH, 2003.
- [2] For a collection of applications of ChGs see: R.K. Willardson, E.R. Weber, (Eds.), Semiconducting Chalcogenide Glass III: Applications of Chalcogenide Glasses, Semiconductors and Semimetals, vol. 80. Elsevier Academic Press, 2004.
- [3] (a) J.B. Wachter, K. Chrissafis, V. Petkov, C.D. Malliakas, D. Bilc, Th. Kyratsi, K.M. Paraskevopoulos, S.D. Mahanti, T. Torbrügge, H. Eckert, M.G. Kanatzidis, J. Solid State Chem. 180 (2007) 420;  
(b) S. Stehlik, J. Orava, T. Kohoutek, T. Wagner, M. Frumar, V. Zima, T. Hara, Y. Matsui, K. Ueda, M. Pumera, J. Solid State Chem. 183 (2010) 144;  
(c) C. Smith, J. Jackson, L. Petit, C. Rivero-Baleine, K. Richardson, J. Solid State Chem. 183 (2010) 1891.
- [4] (a) S.R. Elliott, Physics of Amorphous Materials, 2nd edition, Longman Scientific, 1990;  
(b) A. Feltz, Amorphous Inorganic Materials and Glasses, VCH, Weinheim, 1993.
- [5] (a) S.N. Yannopoulos, A.G. Kalampounias, A. Chrissanthopoulos, G.N. Papatheodorou, J. Chem. Phys. 118 (2003) 3197;  
(b) A.G. Kalampounias, S.N. Yannopoulos, G.N. Papatheodorou, J. Chem. Phys. 125 (2006) 164502.
- [6] (a) K. Jackson, A. Briley, S. Grossman, D.V. Porezag, M.R. Pederson, Phys. Rev. B 60 (1999) R14985;  
(b) S. Blaineau, P. Jund, Phys. Rev. B 69 (2004) 064201.
- [7] (a) P. Boolchand, W.J. Bresser, Nature 410 (2001) 1070;  
(b) F. Kyriazis, A. Chrissanthopoulos, V. Dracopoulos, M. Krbal, T. Wagner, M. Frumar, S.N. Yannopoulos, J. Non-Cryst. Solids 355 (2009) 2010.
- [8] P. Krecmer, A.M. Moulin, R.J. Stephenson, T. Rayment, M.E. Welland, S.R. Elliott, Science 277 (1997) 1799.
- [9] (a) A. Schafer, C. Huber, R. Ahlrichs, J. Chem. Phys. 100 (1994) 5829;  
(b) N. Godbout, D.R. Salahub, J. Andzelm, E. Wimmer, Can. J. Chem. 70 (1992) 560.
- [10] Basis sets were obtained from the EMSL Basis Set Exchange Library: D.J. Feller, Comp. Chem. 17 (1996) 1571;  
K.L. Schuchardt, B.T. Didier, T. Elsethagen, L. Sun, V. Gurumoorthi, J. Chase, J. Li, T.L. Windus, J. Chem. Inf. Model. 47 (2007) 1045.
- [11] T. Petkova, B. Monchev, O. Kostadinova, P. Petkov, S.N. Yannopoulos, J. Non-Cryst. Solids 355 (2009) 2063.
- [12] A. Siokou, M. Kalyva, S.N. Yannopoulos, P. Nemeč, M. Frumar, J. Phys. Condens. Matter 18 (2006) 5525.
- [13] M. Kalyva, A. Siokou, S.N. Yannopoulos, P. Nemeč, M. Frumar, J. Phys. Chem. Solids 68 (2007) 906.
- [14] E.J. Smail, G.M. Sheldrick, Acta Crystallogr. B29 (1973) 2014.
- [15] J. Bastow, H.J. Whitfield, J. Chem. Soc., Dalton (1973) 1739.
- [16] M. Ystenes, F. Menzel, W. Brockner, Spectrochim. Acta A 50 (1994) 225.
- [17] W. Bues, M. Somer, W. Brockner, Z. Anorg. Allg. Chem. 499 (1983) 7.
- [18] W. Bues, M. Somer, W. Brockner, Z. Naturforsch. 35b (1980) 1063.
- [19] A.V. Kolobov, S.R. Elliot, Philos. Mag. B71 (1995) 1.
- [20] K.K. Irikura, R.D. Johnson, R.N. Kacker, J. Phys. Chem. A 109 (2005) 8430.
- [21] S.N. Yannopoulos, M.L. Trunov, Phys. Status Solidi B 246 (2009) 1773.
- [22] A.L. Renninger, B.L. Averbach, Phys. Rev. B 8 (1973) 1507.
- [23] A.J. Leadbetter, A.J. Apling, J. Non-Cryst. Solids 15 (1974) 250.
- [24] S.R. Elliott, A.V. Kolobov, Philos. Mag. B 61 (5) (1990) 853.
- [25] V. Mastelaro, H. Dexpert, S. Benazeth, O.R. Ollitrault-Fichet, J. Solid State Chem. 96 (1992) 301.
- [26] G. Lucovsky, F.L. Galeener, R.H. Geils, R.C. Keezer, in: P.H. Gaskell (Ed.), The Structure of Non-Crystalline Materials, Taylor & Francis, New York, 1977, pp. 127–130.
- [27] S. Onari, O. Sugino, M. Kato, T. Arai, Jpn. J. Appl. Phys. 21 (1982) 418.
- [28] T. Wagner, S.O. Kasap, Philos. Mag. B 74 (1996) 667.
- [29] D.G. Georgiev, P. Boolchand, M. Micoulaut, Phys. Rev. B 62 (2000) R9228.
- [30] T. Petkova, P. Petkov, P. Jovari, I. Kaban, W. Hoyer, A. Schops, A. Webbe, B. Beuneu, J. Non-Cryst. Solids 353 (2007) 2045.
- [31] J.S. Lannin, Phys. Rev. B 15 (1977) 3863.
- [32] T. Usuki, S. Saito, K. Nakajima, O. Uemura, Y. Kameda, T. Kamiyama, M. Sakurai, J. Non-Cryst. Sol. 312 (2002) 570.
- [33] M. Ishii, H. Wada, Mater. Res. Bull. 28 (1993) 1269.
- [34] R.J.H. Clark, D.M. Rippon, J. Mol. Spectrosc. 52 (1974) 58.
- [35] H. Stammreich, R. Forneris, Y. Tavares, J. Chem. Phys. 25 (1956) 580.